ICAS-98-2,6,3

SMALL DISTURBANCE EULER EQUATIONS (SDEE) AN EFFICIENT AND ACCURATE TOOL FOR UNSTEADY LOAD PREDICITIONS AT ALL MACH NUMBERS

Dipl.-Ing. Erich Kreiselmaier
o. Prof. Dr.-Ing. Boris Laschka
Lehrstuhl für Fluidmechanik, Technische Universität München
Boltzmannstr. 15, D-85747 Garching, Germany

Abstract

A numerical method is presented to predict unsteady loads for aeroelastic calculations. It is well known that the time-accurate solutions of the unsteady Euler equations are a reasonable but expensive and time consuming approach, especially for transonic flows. An alternative approach are the small disturbance Euler equations (SDEE) applied to harmonic motion providing the following advantages:

- The unsteady problem is formally reduced to a steady one for the perturbation.
- The first harmonics of unsteady loads are evaluated directly by that supporting the use of well proven modal methods in aeroelastic analysis.
- Substantial reduce of computational time

For an optimal evaluation of the airfoil boundary conditions a harmonically deforming grid is used. Results will be presented for several airfoils and wings in pitching motion at subsonic, transonic and supersonic Mach numbers. It is shown that for the most critical region, namely the transonic region SDEE provides an excellent and relatively quick mean for the prediction of unsteady forces. The only remarkable differences between the exact Euler solution and SDEE solution may be observed at the pressure distribution in the vicinity of the shock, which is of negligible influence for the coefficients.

Nomenclature

Symbols

$\mathbf{A}$	Jacobian matrix (ξ-direction)
c	speed of sound ($\sqrt{\kappa\frac{p}{\rho}}$)
c	chord length
c_r	root chord length
c_t	tip chord length
C_P	pressure coefficient
C_L	lift coefficient
C_M	moment coefficient (about x_m)
d	thickness
e	total energy per unit volume
$\mathbf{F}$, $\mathbf{G}$, $\mathbf{H}$	flux in ξ-, η- and ζ-direction
J	Jacobian of coordinate transformation
k	frequency
k_{red}	reduced frequency ($\frac{k}{\sqrt{\kappa}Ma_\infty}$)
$\mathbf{L}$	matrix of the left eigenvectors
M_∞	freestream mach number
p	pressure
$\mathbf{q}$	conservative solution vector
$\mathbf{Q}$	conservative solution vector times J
$\mathbf{R}$	matrix of the right eigenvectors
$\mathbf{R}$	right hand side
s	half span
$\mathbf{S}$	source term
u, v, w	velocity in x, y and z-direction
U, V, W	contravariant velocities
U^*, V^*, W^*	contravariant velocities times J
V	Volume
x_p	pitching axis
x_m	axis of reference
α	angle of attack
γ	ratio of specific heats
δ	small value
λ	taper ratio
Λ	aspect ratio
Λ	diagonal matrix of eigenvalues
ξ, η, ζ	curvilinear coordinates
ρ	density
τ	time
τ_s	$\sqrt{\kappa}Ma_\infty\tau$
ϕ	sweep angle
Ψ^*	entropy correction parameter
Ψ	limiter function

Superscript

$\bar{}$	mean value
$\tilde{}$	perturbation value
L	left value
R	right value

Subscript

k, l, m	grid index system
0	mean value
1	amplitude

21st ICAS Congress
13-18 September 1998
Melbourne, Australia

Introduction

The ability to predict unsteady loads for aeroelastic calculations in an accurate and economic way is generally a big demand of A/C industry, especially with respect to the development of future ultra high capacity aircrafts. Due to the reduced stiffness of the structure aeroelastic issues play an important role already in the early design phase. Modern CFD-codes based on the solution of the time-accurate solutions of the unsteady Euler- or Navier-Stokes-Equations are successfully applied in the process of aircraft development to investigate the complex aerodynamics, in particular in the transonic region. With respect to aeroelastic applications, where a big number of parameters like different natural modes, angles of attack, Mach numbers, frequencies, etc., must be investigated, such an approach is expensive. In particular simulations at lower frequencies are time consuming, because the periodic state is reached only after a number of cycles nearly independent of frequency.

An alternative approach are the small disturbance Euler equations (SDEE), applied to harmonic motion yielding to a set of linear variable coefficient equations for the complex amplitude of the field quantities. Within this approach first a steady state of reference is calculated with means of the nonlinear Euler equations. Secondly the SDEE describing the unsteady perturbation of the flow are solved. They are based here on an explicit harmonic perturbation but any other time law can be looked at, too. By that the solution of an unsteady problem is formally reduced to a steady one for the perturbation. This leads to an efficient calculation for different frequencies and natural modes based on one steady solution. It is emphasized that the nonlinear flow physics are correctly modelled within the SDEE, because linearization is introduced with respect to time and the only assumption is that the perturbation is small.

Investigations by now on that basis have been done in the field of turbomachinery. Flutter and forced response in twodimensional cascade flows were studied by Hall [3], Hall and Crawley [7], Hall and Clark [4, 5, 14] and Holmes und Chuang [10]. Quasi-threedimensional calculations have been performed by Zirkelbach [21], Kahl and Klose [13], furtheron threedimensional calculations by Hall und Lorence [8] and Hall, Clark und Lorence [6]. The methods proposed exhibit two major differences:

- Modelling of the shock with Shock Fitting or Shock Capturing.
- Evaluation of the airfoil boundary condition based on a deforming grid or a fixed grid.

For the first time Lindquist [18], as well as Lindquist and Giles [17, 19] clarified the crucial question, to what extent the linearized Euler equations can be applied to flows with shocks. Furtheron their investigations of onedimensional nozzle flows proved the successfull application of Shock Capturing. This formed the basis for the calculation of threedimensional flows. The correct modelling of the shock impulse with respect to position and strength is evident due to the fact that the impact on unsteady loads is of the same order than the unsteady pressure distribution in the mainly linear region of the flow field around the airfoil or wing. It was shown that by use of Shock Capturing the shock impulse is smeared out and that the width and the height of the impulse depends on the amount of dissipation of the numerical scheme. But nervertheless its contribution to the unsteady loads does not depend on this effect [6, 18].

The evaluation of the airfoil boundary condition seemed to be a crucial issue for the quality of the results. Under the assumption that an airfoil deforms with small amplitudes it was reasonable to model the moving airfoil with a modified boundary condition and a fixed grid. This boundary condition needs the evaluation of the gradient of the mean flow velocity, which is difficult to compute accurately and leads to significant errors. Hence, this evaluation was discarded by some authors, though it is of great influence at the leading and trailing edge [3, 7, 13, 21]. This deficiency leads to the concept of deforming grids and as consequence to a more complicated formulation of the linearized Euler equations.

The need for an improved method for aeroelastic calculations with consideration of nonlinear effects in the transonic region suggests itself to use the linearized Euler equations in the field of aerodynamics of aircrafts. Therefore at the Lehrstuhl für Fluidmechanik at the Technische Universität München (FLM-TUM) the development of a CFD-code based on the linearized Euler equations was started. Shock Capturing is used due to its inherent simplicty for the nonlinear as well as for the linearized Euler equations. This is accomplished with flux difference splitting after Roe and a modified MUSCL-extrapolation* retaining the TVD-property**. The concept of deforming grids serves for an optimal evaluation of the airfoil boundary condition.

Firstly, investigations for several airfoils (NACA0012, NACA64A010, 3% Parabolic) in pitching motion at subsonic, transonic and supersonic Mach numbers are undertaken. Results will be compared with those gained by a nonlinear Euler method [16] and in the subsonic case additionally with those of an unsteady

*Monotonic Upstream Scheme for Conservation Laws
**Total Variation Diminishing

Kreiselmaier

panel method [11]. Secondly, the application of the method to threedimensional flows is shown, even coping with complicated shock structures. This is done for the well known test case AGARD CT5 *LANN-wing in pitching motion*, which has been used for validition purposes in the framework of the *European Computational Aerodynamics Research Project* (ECARP) [2].

Theory

Euler Equations

In the present analysis, the unsteady, compressible flow around airfoils and wings is modelled as threedimensional, inviscid and adiabatic. Then the governing equations are the threedimensional Euler equations and may be expressed in strong conservation form and curvilinear coordinates for moving grids as

$$\frac{\partial \mathbf{Q}}{\partial \tau} + \frac{\partial \mathbf{F}}{\partial \xi} + \frac{\partial \mathbf{G}}{\partial \eta} + \frac{\partial \mathbf{H}}{\partial \zeta} = 0 \tag{1}$$

in which $\mathbf{Q}$ is the vector of conserved variables times J and $\mathbf{F}$, $\mathbf{G}$ and $\mathbf{H}$ are the convective fluxes with respect to the ξ-, η- and ζ-direction. They are given by

$$\mathbf{Q}=J\mathbf{q}=J\begin{bmatrix}\rho\\ \rho u\\ \rho v\\ \rho w\\ e\end{bmatrix} \qquad \mathbf{F}=J\begin{bmatrix}\rho U\\ \rho uU+\xi_x p\\ \rho vU+\xi_y p\\ \rho wU+\xi_z p\\ U(e+p)-\xi_t p\end{bmatrix}$$

$$\mathbf{G}=J\begin{bmatrix}\rho V\\ \rho uV+\eta_x p\\ \rho vV+\eta_y p\\ \rho wV+\eta_z p\\ V(e+p)-\eta_t p\end{bmatrix} \qquad \mathbf{H}=J\begin{bmatrix}\rho W\\ \rho uW+\zeta_x p\\ \rho vW+\zeta_y p\\ \rho wW+\zeta_z p\\ W(e+p)-\zeta_t p\end{bmatrix}$$

with U, V, W as the contravariant velocities calculated from

$$\begin{aligned} U &= \xi_x u + \xi_y v + \xi_z w + \xi_t \\ V &= \eta_x u + \eta_y v + \eta_z w + \eta_t \\ W &= \zeta_x u + \zeta_y v + \zeta_z w + \zeta_t \end{aligned} \tag{2}$$

Assuming a perfect gas the necessary closing condition is given by the equation of state

$$p = (\kappa - 1)\left[e - \frac{1}{2}\rho\left(u^2 + v^2 + w^2\right)\right] \qquad \text{with } \kappa = \frac{c_p}{c_v} \tag{3}$$

The contravariant metrics are defined by

$$\begin{aligned} J\xi_x &= y_\eta z_\zeta - z_\eta y_\zeta \ , & J\eta_x &= z_\xi y_\zeta - y_\xi z_\zeta \\ J\xi_y &= z_\eta x_\zeta - x_\eta z_\zeta \ , & J\eta_y &= x_\xi z_\zeta - z_\xi x_\zeta \\ J\xi_z &= x_\eta y_\zeta - y_\eta x_\zeta \ , & J\eta_z &= x_\zeta y_\xi - y_\zeta x_\xi \\ J\zeta_x &= y_\xi z_\eta - z_\xi y_\eta \ , & \xi_t &= -x_\tau \xi_x - y_\tau \xi_y - z_\tau \xi_z \\ J\zeta_y &= x_\eta z_\xi - z_\eta x_\xi \ , & \eta_t &= -x_\tau \eta_x - y_\tau \eta_y - z_\tau \eta_z \\ J\zeta_z &= x_\xi y_\eta - y_\xi x_\eta \ , & \zeta_t &= -x_\tau \zeta_x - y_\tau \zeta_y - z_\tau \zeta_z \end{aligned} \tag{4}$$

$$\begin{aligned} J &= x_\xi J\xi_x + y_\xi J\xi_y + z_\xi J\xi_z \\ &= x_\xi(y_\eta z_\zeta - z_\eta y_\zeta) \\ &\quad - y_\xi(x_\eta z_\zeta - z_\eta x_\zeta) + z_\xi(x_\eta y_\zeta - y_\eta x_\zeta) \end{aligned} \tag{5}$$

This forms the basis for a consistent derivation of the linearized Euler equations, being very close to the basic formulation (1). It should be noted that in the framework of a Finite-Volume scheme on structured grids, J denotes the volume of a hexaeder cell, whereas $J\xi_x$, $J\xi_y$ and $J\xi_z$ are the components of the normal cellface vector with respect to the ξ direction and $J\xi_t$ is the change of the volume due to the movement of the cell face.

Linearization

For many aeroelastic calculations the degree of unsteadiness of the flow is small compared to the mean flow. Therefore the flow can be thought of being composed of a steady mean flow and an unsteady small perturbation flow. Furtheron the source of unsteadines is assumed to be harmonic leading to the following formulation for the deforming grid:

$$\begin{aligned} x(\xi,\eta,\zeta,\tau) &= \bar{x}(\xi,\eta,\zeta) + \tilde{x}(\xi,\eta,\zeta)e^{ik\tau} \\ y(\xi,\eta,\zeta,\tau) &= \bar{y}(\xi,\eta,\zeta) + \tilde{y}(\xi,\eta,\zeta)e^{ik\tau} \\ z(\xi,\eta,\zeta,\tau) &= \bar{z}(\xi,\eta,\zeta) + \tilde{z}(\xi,\eta,\zeta)e^{ik\tau} \end{aligned} \tag{6}$$

$\tilde{x}, \tilde{y}, \tilde{z}$ denote the amplitude of grid motion about the steady reference position $\bar{x}, \bar{y}, \bar{z}$ and k is the frequency parameter with respect to the dimensionless time τ. Under these assumptions the metrics of steady state and the metrics of the perturbation, undergoing harmonic variations as well, can be deduced.

$$\begin{aligned} J\xi_x &= \overline{J\xi_x} + \widetilde{J\xi_x}e^{ik\tau} \\ J\xi_y &= \overline{J\xi_y} + \widetilde{J\xi_y}e^{ik\tau} \\ J\xi_z &= \overline{J\xi_z} + \widetilde{J\xi_z}e^{ik\tau} \\ J\xi_t &= \overline{J\xi_t} + \widetilde{J\xi_t}e^{ik\tau} \\ J &= \bar{J} + \tilde{J}e^{ik\tau} \end{aligned} \tag{7}$$

Kreiselmaier

$$\bar{\mathbf{A}} = \begin{bmatrix} 0 & \overline{J\xi_x} & \overline{J\xi_y} & \overline{J\xi_z} & 0 \\ \overline{J\xi_x}\bar{\phi} - \bar{u}\bar{U}^* & \bar{U}^* + (2-\kappa)\overline{J\xi_x}\bar{u} & \overline{J\xi_y}\bar{u} - (\kappa-1)\overline{J\xi_x}\bar{v} & \overline{J\xi_z}\bar{u} - (\kappa-1)\overline{J\xi_x}\bar{w} & (\kappa-1)\overline{J\xi_x} \\ \overline{J\xi_y}\bar{\phi} - \bar{v}\bar{U}^* & \overline{J\xi_x}\bar{v} - (\kappa-1)\overline{J\xi_y}\bar{u} & \bar{U}^* + (2-\kappa)\overline{J\xi_y}\bar{v} & \overline{J\xi_z}\bar{v} - (\kappa-1)\overline{J\xi_y}\bar{w} & (\kappa-1)\overline{J\xi_y} \\ \overline{J\xi_z}\bar{\phi} - \bar{w}\bar{U}^* & \overline{J\xi_x}\bar{w} - (\kappa-1)\overline{J\xi_z}\bar{u} & \overline{J\xi_y}\bar{w} - (\kappa-1)\overline{J\xi_z}\bar{v} & \bar{U}^* + (2-\kappa)\overline{J\xi_z}\bar{w} & (\kappa-1)\overline{J\xi_z} \\ (2\bar{\phi} - \frac{\kappa\bar{e}}{\bar{\rho}})\bar{U}^{**} & (\frac{\kappa\bar{e}}{\bar{\rho}} - \bar{\phi})\overline{J\xi_x} - (\kappa-1)\bar{U}^*\bar{u} & (\frac{\kappa\bar{e}}{\bar{\rho}} - \bar{\phi})\overline{J\xi_y} - (\kappa-1)\bar{U}^*\bar{v} & (\frac{\kappa\bar{e}}{\bar{\rho}} - \bar{\phi})\overline{J\xi_z} - (\kappa-1)\bar{U}^*\bar{w} & \kappa\bar{U}^* \end{bmatrix}$$

$$\bar{U}^* = \overline{J\xi_x}\bar{u} + \overline{J\xi_y}\bar{v} + \overline{J\xi_z}\bar{w}\,, \quad \bar{\phi} = \frac{\kappa-1}{2}(\bar{u}^2 + \bar{v}^2 + \bar{w}^2)$$

For the sake of simplicity this is shown only for the perturbation metrics in ξ-direction.

$$\begin{aligned} \widetilde{J\xi_x} &= \bar{y}_\eta \tilde{z}_\zeta - \bar{z}_\eta \tilde{y}_\zeta + \tilde{y}_\eta \bar{z}_\zeta - \tilde{z}_\eta \bar{y}_\zeta \\ \widetilde{J\xi_y} &= \bar{z}_\eta \tilde{x}_\zeta - \bar{x}_\eta \tilde{z}_\zeta + \tilde{z}_\eta \bar{x}_\zeta - \tilde{x}_\eta \bar{z}_\zeta \\ \widetilde{J\xi_z} &= \bar{x}_\eta \tilde{y}_\zeta - \bar{y}_\eta \tilde{x}_\zeta + \tilde{x}_\eta \bar{y}_\zeta - \tilde{y}_\eta \bar{x}_\zeta \\ \widetilde{J\xi_t} &= -ik\tilde{x}\overline{Jk_x} - ik\tilde{y}\overline{Jk_y} - ik\tilde{z}\overline{Jk_z} \\ \tilde{J} &= \bar{x}_\xi \widetilde{J\xi_x} + \bar{y}_\xi \widetilde{J\xi_y} + \bar{z}_\xi \widetilde{J\xi_z} \\ &\quad + \tilde{x}_\xi \overline{J\xi_x} + \tilde{y}_\xi \overline{J\xi_y} + \tilde{z}_\xi \overline{J\xi_z} \end{aligned} \tag{8}$$

In a similar way the unsteady field quantities are defined by superposition of a steady and a perturbation state:

$$\mathbf{q}(\xi,\eta,\zeta) = \bar{\mathbf{q}}(\xi,\eta,\zeta) + \tilde{\mathbf{q}}(\xi,\eta,\zeta)e^{ik\tau} \tag{9}$$

Now the perturbation expressions of the grid, the metrics and the field quantities are substituted into the Euler equations in strong conservation form and curvilinear coordinates (1). Collecting the terms of zeroth order leads to the nonlinear steady state Euler equations, equivalent to the steady version of equation (1) and every quantity signed by a $\bar{}$. Collecting the terms of first order results after some manipulation in the Small Disturbance Euler Equations (SDEE):

$$\begin{aligned} &\frac{\partial \tilde{\mathbf{Q}}^{(1)}}{\partial\tau} + \frac{\partial \tilde{\mathbf{F}}^{(1)}}{\partial\xi} + \frac{\partial \tilde{\mathbf{G}}^{(1)}}{\partial\eta} + \frac{\partial \tilde{\mathbf{H}}^{(1)}}{\partial\zeta} = \\ &-\left(\tilde{\mathbf{Q}}^{(1)}ik + \tilde{\mathbf{Q}}^{(2)}ik + \frac{\partial \tilde{\mathbf{F}}^{(2)}}{\partial\xi} + \frac{\partial \tilde{\mathbf{G}}^{(2)}}{\partial\eta} + \frac{\partial \tilde{\mathbf{H}}^{(2)}}{\partial\zeta}\right) \end{aligned} \tag{10}$$

$$\tilde{\mathbf{Q}}^{(1)} = \bar{J}\tilde{q} = \begin{bmatrix} \bar{J}\tilde{\rho} \\ \bar{J}\widetilde{\rho u} \\ \bar{J}\widetilde{\rho v} \\ \bar{J}\widetilde{\rho w} \\ \bar{J}\tilde{e} \end{bmatrix} \quad \tilde{\mathbf{F}}^{(1)} = \left.\frac{\partial \mathbf{F}}{\partial \mathbf{q}}\right|_{\bar{\mathbf{q}}} = \bar{\mathbf{A}}\tilde{\mathbf{q}}$$

$$\tilde{\mathbf{Q}}^{(2)} = \begin{bmatrix} \tilde{J}\bar{\rho} \\ \tilde{J}\overline{\rho u} \\ \tilde{J}\overline{\rho v} \\ \tilde{J}\overline{\rho w} \\ \tilde{J}\bar{e} \end{bmatrix} \quad \tilde{\mathbf{F}}^{(2)} = \begin{bmatrix} \bar{\rho}\tilde{U}^* \\ \overline{\rho u}\tilde{U}^* + \widetilde{J\xi_x}\bar{p} \\ \overline{\rho v}\tilde{U}^* + \widetilde{J\xi_y}\bar{p} \\ \overline{\rho w}\tilde{U}^* + \widetilde{J\xi_z}\bar{p} \\ \tilde{U}^*(\bar{e}+\bar{p}) - \widetilde{J\xi_t}\bar{p} \end{bmatrix}$$

$$\tilde{U}^* = \widetilde{J\xi_x}\bar{u} + \widetilde{J\xi_y}\bar{v} + \widetilde{J\xi_z}\bar{w} + \widetilde{J\xi_t} \tag{11}$$

The first term of equation (10) is due to the fact that the perturbation amplitude $\tilde{\mathbf{q}}$ is assumed to be formally time dependent. Hence one obtains a time dependent numerical scheme that is characterized by pseudo time marching. Homogenous terms in $\tilde{\mathbf{q}}$ are marked with $^{(1)}$, inhomogenous terms with $^{(2)}$. It is obvious from the above equations, that an unsteady solution can only be initiated by the unsteady metrics in the inhomogenous terms by causing an interaction of the real and imaginary part of the SDEE. This interaction is removed in the quasisteady case, i.e. $k = 0$. Finally the linearized equation of state is given by

$$\begin{aligned} \tilde{p} = (\kappa-1)\Big[\tilde{e} - \frac{1}{2}\big(&2\bar{u}\widetilde{\rho u} - \bar{u}^2\tilde{\rho} \\ &+2\bar{v}\widetilde{\rho u} - \bar{v}^2\tilde{\rho} + 2\bar{w}\widetilde{\rho u} - \bar{w}^2\tilde{\rho}\big)\Big] \end{aligned} \tag{12}$$

Kreiselmaier

Numerical procedure

Firstly a grid for the mean flow is generated by means of elliptic grid generation as well as a grid that represents the perturbation due to a given deformation of the surface. Secondly the mean flow is computed using a finite volume approach relying on Roe's flux difference splitting. Second order accuracy is achieved by MUSCL exptrapolation, also ensuring the TVD property. With respect to linearization the conservative variables are choosen for extrapolation. Time integration is based on the method of lines allowing the application of different explicit and implicit methods. Especially for threedimensional calculations the LU-SSOR [†] scheme, for the first time introduced by Jameson and Turkel [12], is used.

The SDEE (10) are with the exception of a source term formally equivalent to the original Euler equations (1), resulting in a similar derivation of the discretized equations. Therefore the SDEE are replaced by the following semi-discretized equation,

$$\begin{aligned}
\frac{\partial \tilde{\mathbf{Q}}^{(1)}_{k,l,m}}{\partial \tau} &= -\tilde{\mathbf{R}}_{k,l,m} \\
\tilde{\mathbf{R}}_{k,l,m} &= \tilde{\mathbf{F}}^{(1)}_{k+1/2,l,m} - \tilde{\mathbf{F}}^{(1)}_{k-1/2,l,m} \\
&\quad + \tilde{\mathbf{G}}^{(1)}_{k,l+1/2,m} - \tilde{\mathbf{G}}^{(1)}_{k,l-1/2,m} \\
&\quad + \tilde{\mathbf{H}}^{(1)}_{k,l,m+1/2} - \tilde{\mathbf{H}}^{(1)}_{k,l,m-1/2} \\
&\quad - \tilde{\mathbf{S}}^{(1)}_{k,l,m} - \tilde{\mathbf{S}}^{(2)}_{k,l,m} \\
\tilde{\mathbf{Q}}^{(1)}_{k,l,m} &= \bar{V}_{k,l,m} \tilde{\mathbf{q}}_{k,l,m}
\end{aligned} \tag{13}$$

where $\tilde{\mathbf{S}}^{(1)}_{k,l,m}$ is the homogenous and $\tilde{\mathbf{S}}^{(2)}_{k,l,m}$ is the inhomogenous part of the source term

$$\begin{aligned}
\tilde{\mathbf{S}}^{(1)}_{k,l,m} &= -\tilde{\mathbf{Q}}^{(1)}_{k,l,m} ik \\
\tilde{\mathbf{S}}^{(2)}_{k,l,m} &= -\Big(\tilde{\mathbf{Q}}^{(2)}_{k,l,m} ik \\
&\quad + \tilde{\mathbf{F}}^{(2)}_{k+1/2,l,m} - \tilde{\mathbf{F}}^{(2)}_{k-1/2,l,m} \\
&\quad + \tilde{\mathbf{G}}^{(2)}_{k,l+1/2,m} - \tilde{\mathbf{G}}^{(2)}_{k,l-1/2,m} \\
&\quad + \tilde{\mathbf{H}}^{(2)}_{k,l,m+1/2} - \tilde{\mathbf{H}}^{(2)}_{k,l,m-1/2} \Big)
\end{aligned} \tag{14}$$

The main focus is in the consistent deduction of a linearized Roe flux difference splitting, that is obtained within two steps. The numerical flux $\tilde{\mathbf{F}}^{(1)}_{k+1/2}$ [‡] is given by

$$\begin{aligned}
&\tilde{\mathbf{F}}^{(1)}_{k+1/2} = \\
&\frac{1}{2}\Big[\Big(\mathbf{A}^{(1)\,L}_{k+1/2} + \mathbf{R}^{(1)}_{k+1/2} \left|\bar{\Lambda}_{k+1/2}\right| \mathbf{L}^{(1)}_{k+1/2} \Big) \tilde{\mathbf{q}}^{L}_{k+1/2} \\
&+ \Big(\mathbf{A}^{(1)\,R}_{k+1/2} - \mathbf{R}^{(1)}_{k+1/2} \left|\bar{\Lambda}_{k+1/2}\right| \mathbf{L}^{(1)}_{k+1/2} \Big) \tilde{\mathbf{q}}^{R}_{k+1/2} \Big]
\end{aligned} \tag{15}$$

where $\mathbf{A}^{(1)\,L/R}_{k+1/2}$ are the Jacobian matrices evaluated with the steady state field quantities of the left/right side of the cell interface, however the matrices of the left and right eigenvectors $\mathbf{L}^{(1)}_{k+1/2}$, $\mathbf{R}^{(1)}_{k+1/2}$, as well as the diagonal matrix $\bar{\Lambda}_{k+1/2}$, containing the eigenvalues of the Jacobi matrix $\bar{\mathbf{A}}$, are evaluated with the Roe averages. To maintain consistency to the basic nonlinear Euler solver the eigenvalues are corrected corresponding to Harten [9] and Yee [20] with a continously differentiable approximation of the absolute value function

$$\Psi^*(z) = \begin{cases} |z| & |z| \geq \delta \\ \frac{z^2+\delta^2}{2\delta} & |z| < \delta \end{cases} \tag{16}$$

where δ is a parameter which is obtained by scaling the largest eigenvalue

$$\delta = \delta_1 \cdot \left(|U| + c \left| \vec{\nabla}\xi \right| \right) \tag{17}$$

Furtheron MUSCL-extrapolation is used to calculate the left and right steady state conservative field quantities.

$$\begin{aligned}
\bar{q}^{L}_{k+\frac{1}{2}} &= \bar{q}_k + \frac{1}{2}\bar{\Psi}^{L}_{k+\frac{1}{2}} (\bar{q}_k - \bar{q}_{k-1}) \\
\bar{q}^{R}_{k+\frac{1}{2}} &= \bar{q}_{k+1} + \frac{1}{2}\bar{\Psi}^{R}_{k+\frac{1}{2}} (\bar{q}_{k+2} - \bar{q}_{k+1})
\end{aligned} \tag{18}$$

$$\begin{aligned}
\bar{\Psi}^{L}_{k+\frac{1}{2}} &= \Psi(\bar{r}^{L}_{k+\frac{1}{2}}) \text{ with } \bar{r}^{L}_{k+\frac{1}{2}} = \frac{\bar{q}_{k+1} - \bar{q}_k}{\bar{q}_k - \bar{q}_{k-1}} \\
\bar{\Psi}^{R}_{k+\frac{1}{2}} &= \Psi(\bar{r}^{R}_{k+\frac{1}{2}}) \text{ with } \bar{r}^{R}_{k+\frac{1}{2}} = \frac{\bar{q}_{k+1} - \bar{q}_k}{\bar{q}_{k+2} - \bar{q}_{k+1}}
\end{aligned} \tag{19}$$

For all calculations the Van Albada limiter is used.

$$\Psi = \frac{r^2 + r}{r^2 + 1} \tag{20}$$

Linearizing MUSCL extrapolation up to first order leads to

$$\begin{aligned}
\hat{q}^{L}_{k+\frac{1}{2}} &= \hat{q}_k + \frac{1}{2}\bar{\Psi}^{L}_{k+\frac{1}{2}} (\hat{q}_k - \hat{q}_{k-1}) \\
&\quad + \frac{1}{2}\hat{\Psi}^{L}_{k+\frac{1}{2}} (\bar{q}_k - \bar{q}_{k-1}) \\
\hat{q}^{R}_{k+\frac{1}{2}} &= \hat{q}_{k+1} + \frac{1}{2}\bar{\Psi}^{R}_{k+\frac{1}{2}} (\hat{q}_{k+2} - \hat{q}_{k+1}) \\
&\quad + \frac{1}{2}\hat{\Psi}^{R}_{k+\frac{1}{2}} (\bar{q}_{k+2} - \bar{q}_{k+1})
\end{aligned} \tag{21}$$

[†] Lower-Upper-Symmetric-Successive-Overrelaxation
[‡] For the sake of clarity threefold indexing is omitted

Kreiselmaier

including a perturbation of the limiter. To maintain simplicity and to allow the application of not continously differentiable limiters, the perturbation of the limiter $\hat{\Psi}^{L/R}$ is omitted. Nevertheless a drawback in accuracy is supposed to appear only in regions of strong nonlinearity.

The source term $\tilde{\mathbf{S}}^{(2)}_{k,l,m}$ is computed once at the beginning from the known steady state solution and the perturbation metrics of the prescribed grid motion. The numerical flux $\tilde{\mathbf{F}}^{(2)}$ is

$$\tilde{\mathbf{F}}^{(2)}_{k+1/2} = \frac{1}{2}\left[\tilde{\mathbf{F}}^{(2)}\left(\bar{\mathbf{q}}^{L}_{k+1/2}\right) + \tilde{\mathbf{F}}^{(2)}\left(\bar{\mathbf{q}}^{R}_{k+1/2}\right) - \mathbf{R}^{(2)}_{k+1/2}\left|\tilde{\Lambda}_{k+1/2}\right|\mathbf{L}^{(2)}_{k+1/2}\left(\bar{\mathbf{q}}^{R}_{k+1/2} - \bar{\mathbf{q}}^{L}_{k+1/2}\right)\right] \tag{22}$$

Its important to emphasize that the entropy correction has to be linearized to apply it to the linearized eigenvalues in diagonal matrix $\left|\tilde{\Lambda}_{k+1/2}\right|$.

$$\tilde{\Psi}^{*}\left(\bar{z},\hat{z}\right) = \begin{cases} \frac{\bar{z}}{|\bar{z}|}\hat{z} & |\bar{z}| \geq \delta \\ \frac{\bar{z}}{\delta}\hat{z} & |\bar{z}| < \delta \end{cases} \tag{23}$$

Disregarding this linearization has a strong impact on the quality of the results.

Results

The results are compared with the corresponding nonlinear Euler method and if possible with an unsteady panel method. The different methods are marked with abbreviations throughout all figures. FLMLIN corresponds to the SDEE, FLMEUL to the nonlinear Euler method and POTENTIAL to the above mentioned panel method.

NACA0012 airfoil in pitching motion

The SDEE are first tested for a flow that is governed by linear flow physics. The motion of the airfoil is given by

$$\alpha(\tau_s) = \alpha_0 + \alpha_1 \sin(k_{red} \cdot \tau_s) \tag{24}$$

and the simulation parameters are $Ma_\infty = 0.5$, $k_{red} = 0.0, \ldots, 4.0$, $x_p/c = 0.5$, $x_m/c = 0.5$, $\alpha_0 = 0.0^o$ and $\alpha_1 = 1.0^o$ The Euler calculations were carried out on a fairly coarse C-type grid with 180 cells in the wraparound, 30 cells in the normal direction direction and a farfield distance of 20 chord length. Figure 1 shows the 1. harmonic of the unsteady lift and moment coefficient and figure 2 the corresponding 1. harmonic of the unsteady pressure distribution at two distinct reduced frequencies $k_{red} = 0.5, 2.5$. The agreement between the SDEE and the nonlinear Euler method is excellent for the considered frequency range. A significant difference with increased frequency is observed between the Euler methods and the potential method. This is caused by the different numerical approach which becomes obvious especially at the trailing edge. Euler methods exhibit a certain amount of numerical viscosity leading to an inherent formulation of the Kutta condition and a smooth pressure distribution. In a potential method this has to be done explicitly, leading to a strong recovery of pressure at the trailing edge. Therefore changes are of strong impact on the whole pressure distribution.

NACA64A010 airfoil in pitching motion

To test the capabilities of the present method the well known transonic test case *NACA64A010 airfoil in pitching motion* [1] for which the simulation parameters are given by $Ma_\infty = 0.796$, $k_{red} = 0.05, \ldots, 0.606$, $x_p/c = 0.25$, $x_m/c = 0.25$, $\alpha_0 = 0.0^o$ and $\alpha_1 = 1.0^o$ is considered. Again a C-type grid with the same parameters as above is used. To adapt the grid to the expected flow it is refined in the region of the shock movement. Figure 4 depicts the 0. and 1. harmonic of the pressure distribution. It is noted that C^0_P of the SDEE and experiment are steady state values. With the exception of the shock region the prerequisites of linearization are excellent. The agreement with experimental results is extremely good in the shock region and downstream. Differences for C^0_P are observed upstream of the shock due to wind tunnel wall effects [15]. The numerical evaluated lift and moment coefficients in figure 3 agree very well. This is amazing because shock movement covers a region of about 20% of the chord length depending on the frequency. This emphasizes the fact that the 1. harmonic of pressure distribution is different in the shock region for SDEE and nonlinear Euler, however the load contribution of the shock impulses are equal. This verifies the equivalent impact of shock impulses, originally introduced by Lindquist and Giles [17, 19]. Therefore shock-capturing is an appropriate approach even for linearized Euler equations by that opening the way for transonic, threedimensional applications where shock-fitting is too complex. Significant differences in the coefficients can be seen with respect to the experiment that are caused by unsteady shock movement.

3% Parabolic airfoil in pitching motion

In this section SDEE is tested for a supersonic case. The existence of sharp leading and trailing edges implies the use of an H-type grid. Its composed of two

blocks with 120×30 cells each and with 60 cells on every side of the airfoil. The simulation parameters are given by $Ma_\infty = 1.4$, $k_{red} = 0.0, \ldots, 2.0$, $x_p/c = 0.5$, $x_m/c = 0.5$, $\alpha_0 = 0.0^o$ and $\alpha_1 = 1.0^o$. In this case the shocks are fixed to the leading and trailing edges ensuring an excellent agreement not only for the coefficients (Fig. 5), but also for the unsteady pressure distribution (Fig. 6).

LANN wing in pitching motion

For threedimensional calculations the LANN wing in transonic flow is selected. Within the *European Computational Aerodynamics Research Project* (ECARP) [2] the AGARD CT5 test case is subject to extensive investigations with different CFD codes. Geometric parameters are given by table 1 and the simulation parameters are $Ma_\infty = 0.82$, $k_{red} = 0.0, \ldots, 1.0$, $x_p/c_r = 0.621$, $x_m/c = 0.25$, $\alpha_0 = 0.6^o$ and $\alpha_1 = 0.25^o$.

LANN-*wing*			
s	2.77	c_r	1.0
$\lambda = c_t/c_r$	0.4	Λ	7.92
$\varphi_{0.25}$	25^o	d/c	12%

Table 1: Geometric parameters

The simulation is done on a CH-type grid with $160 \times 32 \times 40$ cells that is suggested by ECARP. Lower and upper surface exhibit 60×28 cells. The upper side of the wing shows the λ-shocksystem (Fig. 8). Figure 7 depicts the unsteady lift and moment coefficient for the considered range of frequency. The agreement of SDEE and nonlinear Euler is excellent even for a complicated shock structure. This is confirmed by a closer look at the unsteady pressure distribution at two different spanwise sections (Figs. 8, 9, 10). The 0. harmonic of pressure exhibits an excellent agreement at the section $y/s = 32.5\%$ even in the shock region, because recompression is done within two shocks whose strength is weaker and more smooth compared to the single shock at section $y/s = 65.0\%$. At this section a significant difference is only seen at the shock. This states that with the exception of the shock region the flow physics are linear. Also shown are computational results from two ECARP partners:

- DLR [††] Institute of Aeroelasticity (DLR AE)
- DLR Institute of Design Aerodynamics (DLR EA)

A shock displacement of about 2% due to different amounts of numerical viscosity is observed at the first shock of the inner section, but overall agreement with these results is very good. The 1. harmonics of pressure distribution of SDEE and nonlinear Euler agree very well. As in the twodimensional case the shock impulse exhibts some difference, but contribution to the unsteady load is equal. With respect to the results of DLR EA and DLR AE differences occur not only at the shocks. The displacement of the first shock impulse at section $y/s = 32.5\%$ corresponds to the displacement of the shock. Figure 10 shows clearly that the differences in the computational results due to numerical modelling are more significant than the differences obtained with the linearized or nonlinear Euler method. It is emphasized that in the present study the SDEE use one tenth the time of the corresponding nonlinear Euler solver.

Conclusions

A new consistent linearization of the unsteady, threedimensional nonlinear Euler equations is presented. This leads to a set of linear variable coefficient equation called SDEE (Small Disturbance Euler Equations). The validity of the approach was shown for several airfoils and wings in pitching motion at subsonic, transonic and supersonic Mach numbers. For a NACA0012 airfoil in pitching motion at $Ma = 0.5$ it is shown that the agreement between SDEE and nonlinear Euler is excellent. The most critical case is the transonic flow. This case has been studied for a NACA64A010 airfoil and the LANN-wing in pitching motion. It confirms the equivalent impact of shock impulses, originally introduced by Lindquist and Giles [17, 19]. It has been proven that SDEE is an excellent approach for unsteady transonic flows even in the case of complex shock strutures. The application of SDEE is less critical for supersonic flows around airfoils with sharp leading and trailing edges due to the fixed shocks. Furthermore it reduces computational time by a factor of ten.

Work is underway to determine the limits of the SDEE with respect to amplitudes of motion, shock movement and strength. The present approach will be used in the framework of aeroelastic calculations of threedimensional configurations.

[††] Deutsches Zentrum für Luft- und Raumfahrt

Kreiselmais.

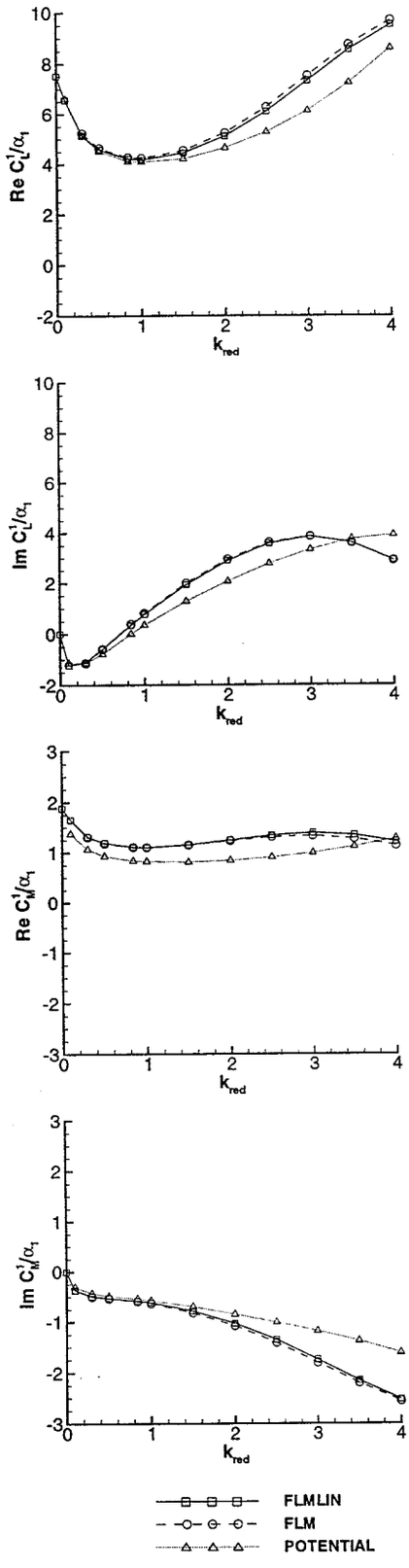

Figure 1: NACA0012: Real and imaginary part of 1. harmonic of C_L and C_M at $Ma_\infty = 0.5$

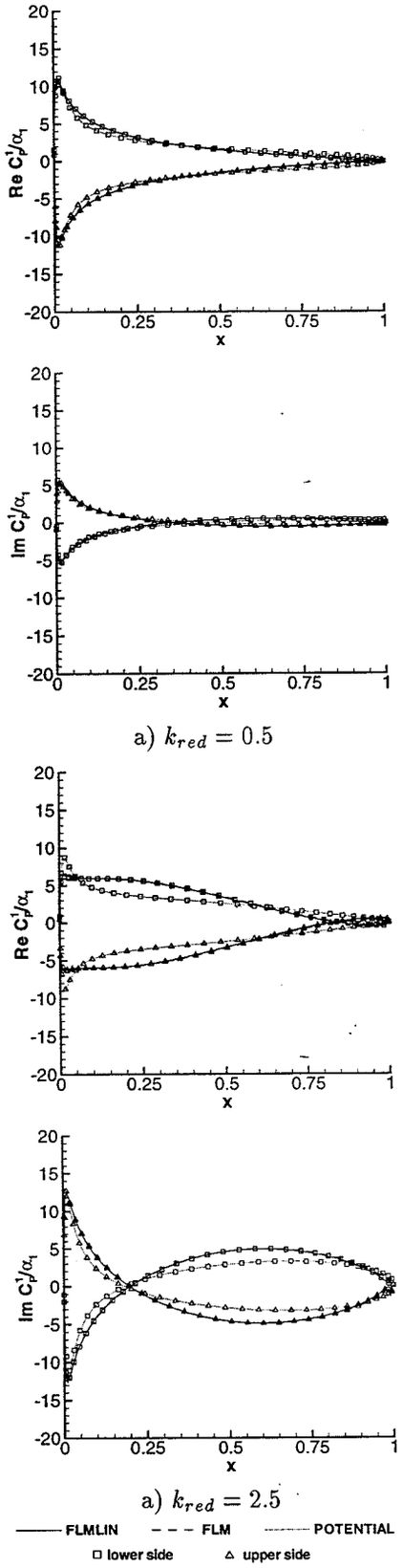

Figure 2: NACA0012: ReC_P^1 und ImC_P^1 at reduced frequency $k_{red} = 0.5,\ 2.5$

Kreiselmaier

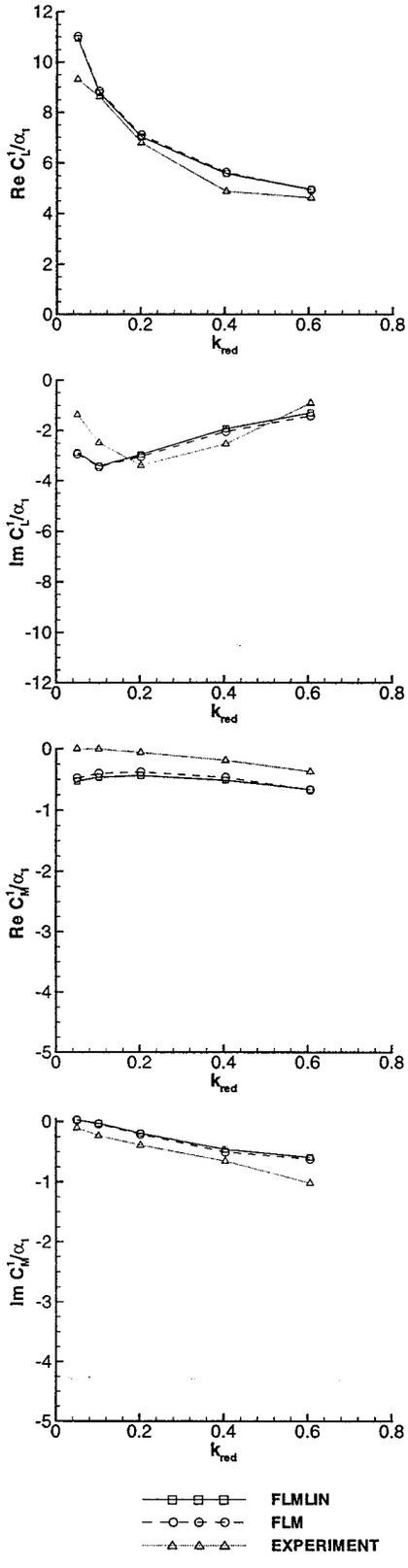

Figure 3: NACA64A010: Real and imaginary part of 1. harmonic of C_L and C_M at $Ma_\infty = 0.796$

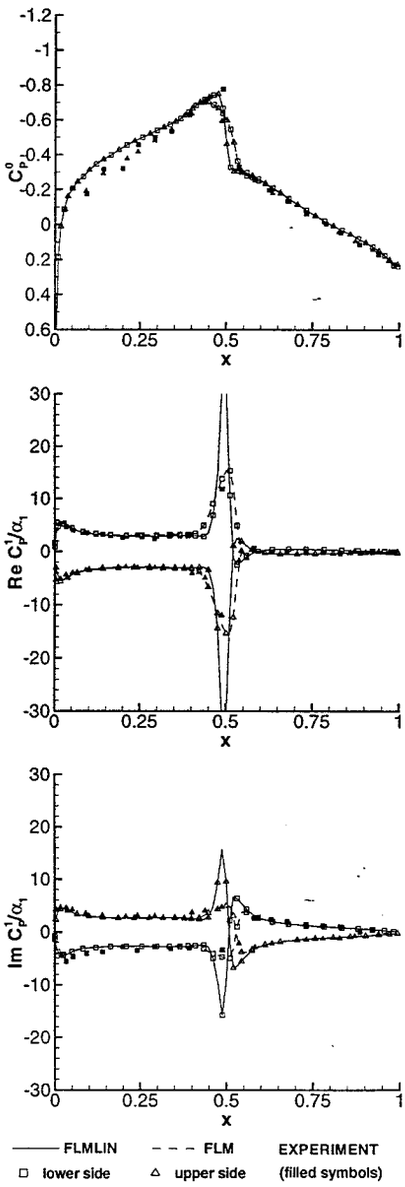

Figure 4: NACA64A010: C_P^0, ReC_P^1 und ImC_P^1 at reduced frequency $k_{red} = 0.404$

Kreiselmaier

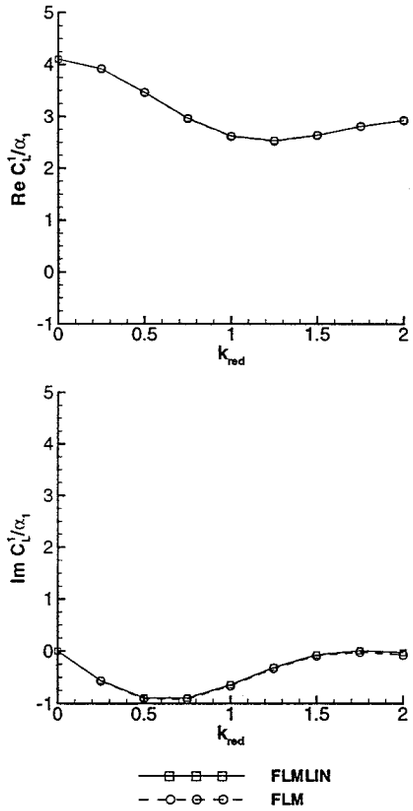

Figure 5: 3% Parabolic: Real and imaginary part of 1. harmonic of C_L at $Ma_\infty = 1.4$

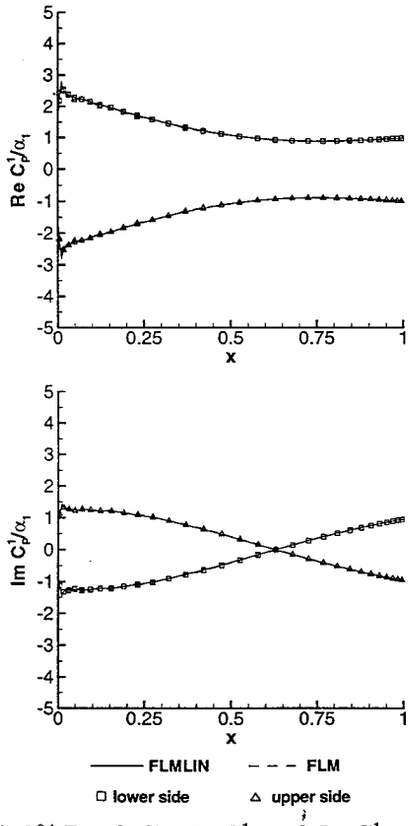

Figure 6: 3% Parabolic: ReC_P^1 und ImC_P^1 at reduced frequency $k_{red} = 1.0$

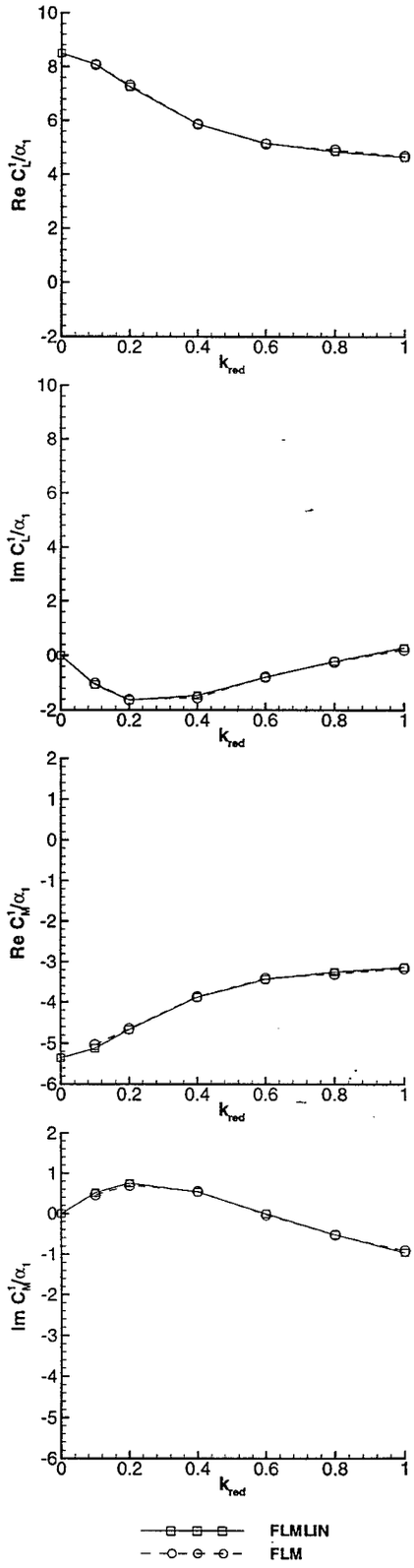

Figure 7: LANN-wing: Real and imaginary part of 1. harmonic of C_L and C_M at $Ma_\infty = 0.82$

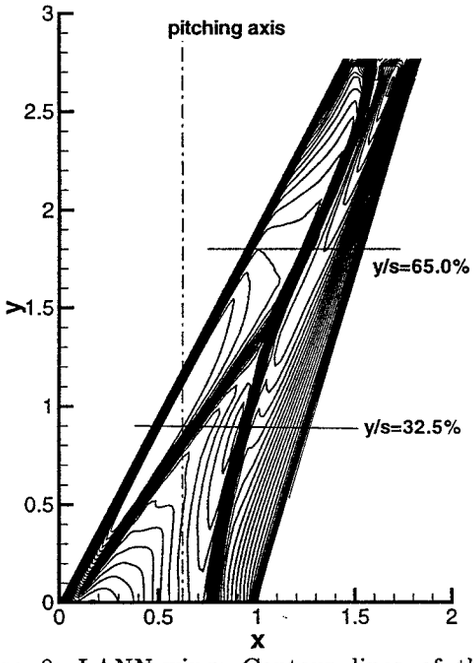

Figure 8: LANN-wing: Contour lines of the C_P-distribution on the upper surface of the wing ($\Delta C_P = 0.025$)

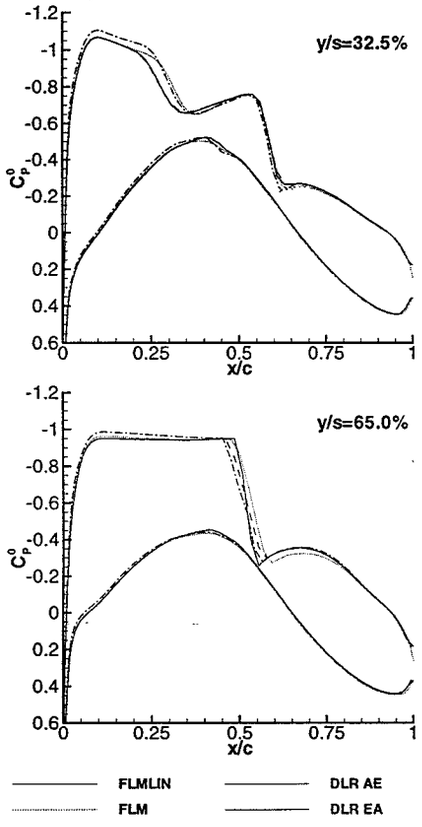

Figure 9: LANN-wing: C_P^0 at reduced frequency $k_{red} = 0.206$

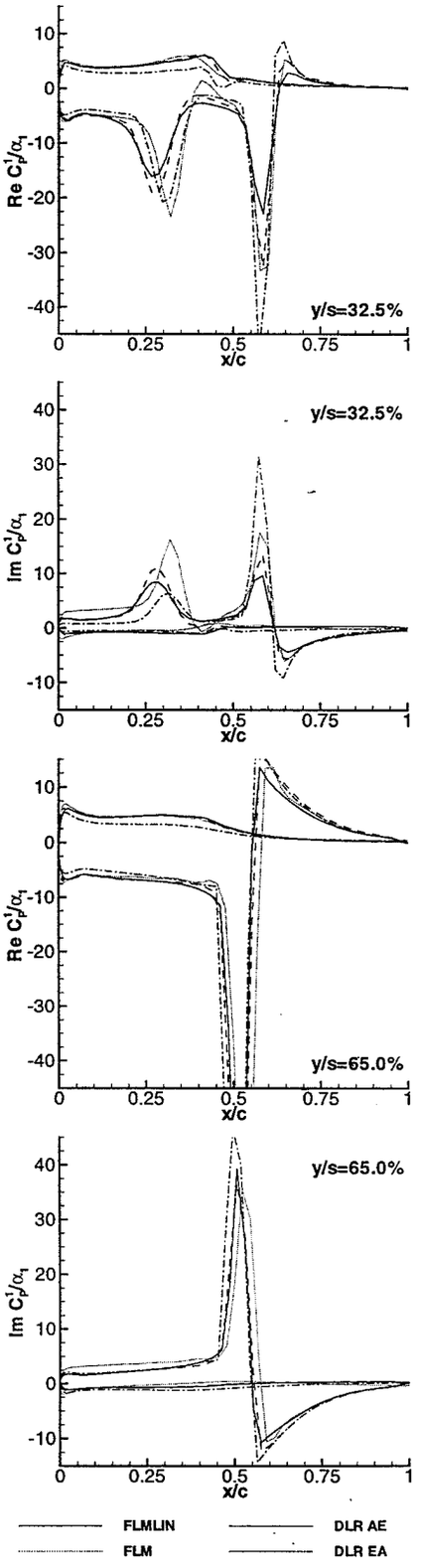

Figure 10: LANN-wing: C_P^0 at reduced frequency $k_{red} = 0.206$

Kreiselmaier

References

[1] Sanford S. Davis. NACA64A010 (NASA Ames Model) Oscillatory Pitching, Compendium of Unsteady Aerodynamic Measurements. Technical report, AGARD, 1982. AGARD-R-702.

[2] W. Haase and et. al., editors. *ECARP - European Computational Aerodynamics Research Project: Validation of CFD Codes and Assessment of Turbulence Models.* Vieweg, Braunschweig/Wiesbaden, 1997.

[3] K. C. Hall. *A Linearized Euler Analysis of Unsteady Flows in Turbomachinery.* PhD thesis, Massachusetts Institute of Technology, 1987.

[4] Kenneth C. Hall and William S. Clark. Calculation of Unsteady Linearized Euler Flows in Cascades Using Harmonically Deforming Grids. *Sixth Symposium on Unsteady Aerodynamics and Aeroelasticity of Turbomachines and Propellers, Notre Dame*, 1991.

[5] Kenneth C. Hall and William S. Clark. Prediction of Unsteady Aerodynamic Loads in Cascades using the Linearized Euler Equations on Deforming Grids. *AIAA-91-3378-CP*, 1991.

[6] Kenneth C. Hall, William S. Clark, and Christopher B. Lorence. A Linearized Euler Analysis of Unsteady Transonic Flows in Turbomachinery. *ASME Paper 93-GT-94*, 1992.

[7] Kenneth C. Hall and E. F. Crawley. Calculation of Unsteady Flows in Turbomachinery Using the Linearized Euler Equations. *AIAA*, 27(6):777–787, June 1989.

[8] Kenneth C. Hall and Christopher B. Lorence. Calculation of Three-Dimensional Unsteady Flows in Turbomachinery Using the Linearized Harmonic Euler Equations. *ASME Paper 92-GT-136*, 1992.

[9] A. Harten. On a Class of High Resolution Total-Variation-Stable Finite Difference Schemes. *SIAM Journal of Numerical Analysis*, 21:1–23, 1984.

[10] D. G. Holmes and H. A. Chuang. Twodimensional Linearized Harmonic Euler Flow Analysis for Flutter and Forced Response. *Sixth Symposium on Unsteady Aerodynamics and Aeroelasticity of Turbomachines and Propellers, Notre Dame*, 1991.

[11] Th. Huber and H. Rochholz. Instationäre Strömungen an Tragflächen und Körpern, Kompressible Strömungen. Technical report, TUM, 1990. TUM-LSM 90/66.

[12] A. Jameson and E. Turkel. Implicit Schemes and LU-Decompositions. *Mathematics of Computation*, 37:385–397, 1981.

[13] G. Kahl and A. Klose. Time Linearized Euler Calculations for Unsteady Quasi-3D Cascade Flows. *Sixth Symposium on Unsteady Aerodynamics and Aeroelasticity of Turbomachines and Propellers, Notre Dame*, 1991.

[14] C. Hall Kenneth and William S. Clark. Linearized euler predictions of unsteady aerodynamic loads in cascades. *AIAA*, 31(3):540–550, March 1992.

[15] L. S. King and D. A. Johnson. Calculations of Transsonic Flow about an Airfoil in a Wind Tunnel. *AIAA Paper 80-1366-CP*, 1980.

[16] E. Kreiselmaier. *Berechnung instationärer Tragflügelumströmungen auf der Basis der zeitlinearisierten Eulergleichungen.* PhD thesis, Technische Universität München, 1998.

[17] D. R. Lindquist and M. B. Giles. Validity of linearized unsteady euler equations with shock capturing. *AIAA*, 32(1):46–53, January 1994.

[18] Dana R. Lindquist. *Computation of Unsteady Transonic Flowfields Using Shock Capturing and Linear Perturbation Euler Equations.* PhD thesis, Massachusetts Institute of Technology, 1992.

[19] Dana R. Lindquist and Michael B. Giles. On the validity of linearized unsteady euler equations with shock capturing. *AIAA-91-1598-CP*, 1991.

[20] H. C. Yee. A Class of High Resolution Explicit and Implicit Shock Capturing Methods. Technical report, NASA Ames Research Center, 1989. NASA Technical Memorandum 101088.

[21] J. Zirkelbach. Lösung der zeitlinearisierten Eulergleichungen für schwingende Schaufelgitter in Quasi-3D Strömung. Master's thesis, Technische Universität München, 1990.

Kreiselmaier